Geoscience Frontiers 17 (2026) 102294

Contents lists available at ScienceDirect

Geoscience Frontiers

journal homepage: www.elsevier.com/locate/gsf

Research Paper

Abiotic hydrocarbons via hydromagnesite–FeO redox reactions

Jingqin Xu [a], Yajie Wang [a], Dexiang Gao [b,c], Hao Luo [a], Jie Zhang [a], Yunfan Fei [a], Ruyue Shi [a], Guoliang Niu [a], Ho-kwang Mao [a], Kuo Li [a], Haiyan Zheng [a,*]

[a] Center for High Pressure Science and Technology Advanced Research, Beijing 100193, PR China
[b] Institute of High Energy Physics, Chinese Academy of Sciences, Beijing 100049, PR China
[c] Spallation Neutron Source Science Center, Dongguan 523803, PR China

ARTICLE INFO

Article history:
Received 18 July 2025
Revised 31 December 2025
Accepted 25 February 2026
Available online 26 February 2026

Keywords:
High temperature
High pressure
Abiotic hydrocarbons
Mantle
Hydromagnesite–FeO
Redox reactions

ABSTRACT

Abiotic formation of hydrocarbons within the Earth's deep interior represents a crucial aspect of the global carbon cycle. Understanding the process from carbonates (oxidized state) and hydrocarbons (reduced state), and the compositional distribution of hydrocarbons at various deep-earth pressure–temperature conditions are essential for improving carbon cycling models. Here we studied the chemical reactions among hydromagnesite, H_2O, and FeO under the deep Earth conditions (10–20 GPa, 900–2100 K), employing diamond anvil cell coupled with laser/resistive heating techniques as well as large volume press. The experimental results reveal a progression from saturated to unsaturated hydrocarbons with increasing *P–T* conditions. More importantly, we identified ethanol and acetaldehyde in the recovered product. This indicates that the reduction process of carbonates involves multiple intermediate processes, and complex organic compounds can be stabilized at suitable conditions. Our study provides new insights into the mechanisms of hydrocarbon formation in the deep Earth.

1. Introduction

The storage, conversion and transportation of carbon in the deep Earth is important to understand the processes of the global carbon cycle and predict the production of abiotic oil/gas (Molina and Poli, 2000; Frezzotti et al., 2011; Dasgupta, 2013; Leila et al., 2025a, 2025b). Among these processes, the formation of deep Earth hydrocarbons is the key chemical reaction, and the redox reactions among carbon sources (such as carbonates and diamonds), hydrogen sources (H_2 or H_2O) and reductants (such as FeO) under extremely high pressure and high temperature (HPHT) are highly focused (Kutcherov and Krayushkin, 2010; McCollom, 2013). Over the past two decades, advances in HPHT experiments and thermodynamic modeling have enabled the reconstruction of several abiotic hydrocarbon-forming pathways from carbonates at pressures up to 10–11 GPa and temperatures of 500–1800 °C, broadly corresponding to crustal to upper-mantle depths (<410 km, $P < 11$ GPa) (Wang et al., 2023). This study has demonstrated that CH_4 and C_2–C_5 light alkanes can be synthesized from carbon sources like carbonates, graphite, or CO_2, hydrogen sources like H_2O or H_2, and reductants like FeO or Fe, under reducing conditions consistent with those expected in subducted slabs and upper mantle (Scott et al., 2004; Kutcherov et al., 2013; McCollom, 2013; Wang et al., 2023). Within the Earth's crust (0–30 km), the Fischer-Tropsch reaction ($H_2 + CO_2 \rightarrow CH_4$, $H_2 + CO \rightarrow CH_4$) are widely recognized as a major abiotic methane-forming process in ultramafic and hydrothermal systems (Etiope and Sherwood Lollar, 2013). In the upper mantle, C_1-C_5 was identified in the FeO-$CaCO_3$-H_2O and Fe-$CaCO_3$-H_2O system at 3–11 GPa and 800–1800 K (Kutcherov et al., 2002; Scott et al., 2004; Kutcherov et al., 2010a, 2010b). CH_4 can be produced from graphite-H_2 mixture at 1–8 GPa and 600–1800 K (Sharma et al., 2009). Light hydrocarbons such as CH_4, C_2H_6 and C_3H_8 can be generated from the reaction between iron-bearing dolomite and water under subduction-zone *P–T* conditions, highlighting carbonate reduction as a robust deep source of abiotic hydrocarbons (Tao et al., 2018).

While the generation of abiotic methane have been confirmed in the crust and upper mantle, the generation of hydrocarbon in the transition zone to lower mantle (>410 km) are still not well understood. Usually, this region is considered to be more reductive compared to upper mantle and crust, with abundant hydrogen sources (e.g., H_2O and H_2; Pearson et al., 2014; Hu et al., 2016, 2017; Mao et al., 2017) and carbon sources (e.g., magnesite, diamond, and iron-carbon alloys; Dasgupta and Hirschmann, 2010). In addition to H_2 produced by water–rock interaction and carbon-

* Corresponding author.
E-mail address: zhenghy@hpstar.ac.cn (H. Zheng).

https://doi.org/10.1016/j.gsf.2026.102294

ate reduction, reduced sulfur species such as H_2S and HS^- also represent an important, and often overlooked, hydrogen and electron reservoir in deep fluids. For example, serpentinization and Fe–S–bearing assemblages in ultramafic and subduction environments commonly yield H_2–H_2S-rich fluids, which can buffer redox conditions and participate in hydrocarbon formation or stabilization (McCollom and Bach, 2009; Charlou et al., 2010; Colin et al., 2020; Vitale Brovarone et al., 2020; Farsang and Zajacz, 2024). Although our experimental system is formally S-free, these results indicate that, in natural subduction-zone and mantle-wedge environments, H_2S and HS^--bearing fluids cannot be disregarded in terms of their contribution to hydrogen sources. Collectively, these conditions define a thermodynamically favorable environment for deep abiotic hydrocarbon formation. However, the specific reduction pathways of carbonate phases and the nature of hydrocarbon products under transition-zone to lower-mantle *P–T* conditions are still poorly understood. In addition, experimental studies indicate that lower thermobaric limit for abiotic hydrocarbon formation is on the order of 280–300 °C and 2–3 GPa (Mukhina et al., 2017). Clarifying how carbonates are reduced and how hydrocarbons are generated and transformed under these conditions has thus become a central question for both deep carbon cycling and the potential contribution of deep abiotic hydrocarbons to Earth's long-term carbon budget.

In this work, we investigated the production of abiotic hydrocarbon under the deep-earth condition by subjecting the hydromagnesite ($4MgCO_3{\cdot}Mg(OH)_2{\cdot}4H_2O$)-$H_2O$-FeO system. With increasing temperature and pressure, the hydrocarbon products transform from saturated hydrocarbons (low C/H ratio) to unsaturated hydrocarbons (high C/H ratio). More importantly, ethanol and acetaldehyde were identified as intermediate products, which disclosed a multi-step route for the generation of abiotic hydrocarbon in the deep mantle, and suggests that complex organics can be formed in deep earth at certain conditions.

2. Experimental methods

2.1. High pressure and high temperature experiments

The hydromagnesite ($4MgCO_3{\cdot}Mg(OH)_2{\cdot}4H_2O$, was purchased from Rhawn chemical reagent Co., Ltd.) and ferrous oxide (FeO, 99.6%, was obtained from Innochem) were used without further purification. The two powders were thoroughly mixed in a molar ratio of $4MgCO_3{\cdot}Mg(OH)_2{\cdot}4H_2O$: FeO = 1:8 to ensure homogeneity prior to high-pressure experiments. A series of *in situ* high-pressure experiments, including Raman spectroscopy and laser/resistive heating, were carried out using a symmetric diamond anvil cell (DAC) equipped with 300 μm culet anvils. Prior to sample loading, T301 stainless steel gasket was pre-indented to a thickness of approximately 30 μm, and a central hole with a diameter of 180 μm was drilled to form the sample chamber. Then, the sample was first pre-indented into a flake and then loaded into the DAC. A small amount of water was subsequently added using a micropipette, followed by rapid compression to approximately 1 GPa. Pressure calibration was performed using the ruby fluorescence measurements (Mao et al., 1986). For laser heating experiment, the double-sided laser heating was applied using two 1070 nm ytterbium fiber lasers, and real-time temperature monitoring was achieved through coupled spectrometers. To achieve uniform heating of the samples, resistive heating was employed in high-temperature and high-pressure experiments using a BX90 DAC (300 μm culet), fitted with a custom-designed resistive ring heater encircling the diamond anvils. Temperature measurements were conducted using a K-type thermocouple affixed to the diamond, while pressure was determined through temperature-corrected ruby fluorescence measurements (Rekhi et al., 1999).

High-pressure and high-temperature experiments were conducted using a multi-anvil apparatus: a 20-MN Kawai-type press. We conducted experiments using a 14/8 assembly equipped with a rhenium heater (as shown in Supplementary Data Fig. S1 for schematic details) under approximately 10 GPa. For experiments, sintered MgO octahedra with an edge length of 14 mm were used. Rhenium foil (0.05 mm thick) served as the resistive heating element, while a ZrO_2 sleeve functioned as the thermal insulator. Pressure calibration was performed using known phase transitions in reference materials—including Bi and ZnTe at room temperature (Chen et al., 2016; Song et al., 2021). Temperature was monitored with a W97Re3-W75Re25 (D-type) thermocouple. For all runs, the sample was enclosed in sealed Pd-Au capsules. Prior to loading, the mixed powders were cold-pressed into a cylindrical pellet with a diameter of 2.4 mm and a height of 3.6 mm. The pellet was then placed into the capsule, after which small amount of deionized water was added dropwise. The capsule was subsequently sealed to prevent fluid loss during high temperature and high pressure experiments. Compression to the target pressure was performed incrementally at a rate of ~3 GPa per hour, followed by controlled heating at ~20 °C per minute until the target temperature was reached. After maintaining the pressure for 12 h, samples were quenched by terminating the power supply. Decompression to ambient pressure proceeded gradually at ~2 GPa per hour.

2.2. In situ Raman spectroscopy measurements

In this research, all Raman spectroscopy experiments were performed with a Renishaw Raman microscope (RM1000), equipped with multiple laser sources and interchangeable diffraction gratings: 1800 gr/mm (He–Ne laser, 633 nm), and 2400 gr/mm (Nd:YAG laser, 532 nm). Raman spectra were collected over the range of 50–4000 cm^{-1} using 633 nm and 532 nm excitation lasers. The system was calibrated by the Si line.

2.3. High-resolution gas chromatography (GC)–mass spectrometry (MS) measurement

To analyze the composition of products obtained from the multi-anvil press experiments, a Thermo Scientific™ Q Exactive™ gas chromatography–hybrid quadrupole–Orbitrap mass spectrometer was employed. The solid product generated under high pressure was dissolved in 0.5 mL of dichloromethane (CH_2Cl_2, HPLC purity, 99.9%), with a portion of the samples exhibiting solubility. Sample injection (1 μL) was performed automatically in Split/Splitless (S/SL) mode. To analyze the composition of gaseous products, gas samples were extracted from the quenched Pd-Au capsule using either a steel needle or a crushing apparatus, as shown in Supplementary Data Fig. S2. The entire capsule was positioned within a sealed chamber located directly beneath the steel needle to ensure controlled gas release. Subsequently, a 100 μL gas sample was manually introduced using a gas-tight manual syringe, and the sample was injected into the S/SL injector. Chromatographic separation was achieved using a TG-5SilMS capillary column (30 m × 0.25 mm I.D. × 0.25 μm film thickness), with high-purity helium (99.999%) as the carrier gas at a constant flow rate of 1.0 mL/min. The GC oven was programmed to hold at 40 °C for 2 min, followed by a linear increase to 200 °C at a rate of 5 °C/min. Both the inlet, ion source, and transfer line temperatures were maintained at 200 °C throughout the run. The system utilized an electron ionization (EI) source set at 70 eV, and mass spectra were obtained within the mass-to-charge ratio (m/z) range of 30–450. Data collection was managed via Thermo Scientific™ TraceFinder™ 4.0 software. Mass spectral deconvolution and compound identification were carried out using Thermo Scientific's built-in deconvolution tools, with compound assignments based on spectral matching

against the National Institute of Standards and Technology (NIST) 2014 and Wiley reference libraries, supplemented by high-resolution filtering (HRF) to ensure mass accuracy and confidence in identification.

2.4. In situ high pressure X-ray diffraction (XRD)

In situ high pressure XRD experiments were carried out at the High Pressure Station on beamline 4W2 of the Beijing Synchrotron Radiation Facility (BSRF). A monochromatic X-ray beam with a wavelength of 0.6199 Å was employed, and diffraction patterns were recorded using a Pilatus 2M detector that had been calibrated using a CeO_2 standard. The incident beam was focused to an area of approximately 20 μm × 30 μm. The Dioptas software was employed to facilitate the integration of the acquired two-dimensional XRD patterns (Prescher and Prakapenka, 2015). Rietveld refinement was conducted using the Jana2006 software suite for data analysis to determine the structure and composition of the product, as well as to further investigate the reaction mechanism (Petříček et al., 2014).

3. Results

The laser-heating experiments were performed in a diamond anvil cell (DAC) under three distinct pressure–temperature conditions to simulate geological environments of the transition zone and lower mantle: 12 GPa/(1500–1800 K), 20.9 GPa/(1400–1600 K), and 26.8 GPa /(1700–2100 K), respectively. In all experiments, the sample was first compressed to the target pressure, heated and cooled down to room temperature for Raman experiment. The system remains stable with no chemical reactions occurring up to 27.6 GPa at room temperature, as shown in Supplementary Data Fig. S3, further details are provided in the Supplementary Information.

For the experiment at 1500–1800 K and 12 GPa, after cooling down to room temperature, Raman spectra of the products were collected, as shown in Fig. 1a. At 11.7 GPa, new peaks appeared at 1107 and 1624 cm^{-1}, which are attributed to the stretching vibrational modes of C-C and C=C, respectively (Kudryavtsev et al., 2017; Read et al., 2020; Yamawaki, 2020; Li et al., 2021; Yang et al., 2021; Xu et al., 2025). As the pressure decreases, these peaks are significantly enhanced and remain clearly visible. At 4.0 GPa, a new peak appeared at 2965 cm^{-1}, which are attributed to the stretching vibrational modes of sp^3 C-H. This observation clearly demonstrates the formation of abiotic hydrocarbons, mainly alkanes and olefins. *In situ* high-pressure X-ray diffraction (XRD) pattern of the solid product was analyzed at 1.8 GPa. Rietveld refinement revealed the presence of ε-FeOOH, FeO, MgO, and $Mg(OH)_2$ within the products (Fig. 1b) (Gleason et al., 2008; Thompson et al., 2017). These observations indicate that the reduction of carbonates was accompanied by thermal decomposition of $4MgCO_3{\cdot}Mg(OH)_2{\cdot}4H_2O$ and the oxidization of FeO.

Then we investigated the reaction in transition zone (P = 20.9 GPa, T = 1400–1600 K). The Raman spectra of the products after cooling down to room temperature as shown in Fig. 1c. The pressure increased to 23.8 GPa, a broad band and some new peaks appeared at 1430–1660 and 2800–3250 cm^{-1}, corresponding to the symmetric C=C stretching and the sp^3 C-H and sp^2 C-H stretching mode, respectively (Ward et al., 2018; Li et al., 2021; Xu et al., 2025). Upon decompression, these peaks remain stable to 5.7 GPa. In addition, a distinct peak became obvious at 2078 cm^{-1} at 5.7 GPa, which is attributed to the C≡C stretching vibrational mode (Hirai et al., 2009; Lobanov et al., 2013; Ward et al., 2018; Zhang et al., 2020). These phenomena demonstrate that the system undergoes the redox reactions to form olefins and alkynes. At elevated pressures and temperatures representative of lower mantle conditions (P = 26.8 GPa, T = 1700–2100 K, Fig. 1d), characteristic peaks belonging to the C=C (1440–1680 cm^{-1}) and C≡C (2180 cm^{-1}) stretching mode were also found in the Raman spectra of the products after cooling down to room temperature. Correspondingly, the sp^3 C-H and sp^2 C-H stretching vibrations were observed in 2874, 2987, 3108, 3226 cm^{-1} at 23.7 GPa and remain stable to 5.7 GPa (Hirai et al., 2009; Lobanov et al., 2013; Ward et al., 2018; Li et al., 2021; Xu et al., 2025). Therefore, both alkenes and alkynes are present among the reaction products.

We also conducted resistive heating experiment using a BX90 DAC with T301 stainless steel gasket for comparison, which provides more even pressure and temperature conditions. The experiments were conducted at P = 12.0 GPa and T = 974 K (with a holding time of 2 h) to explore the kinetic thresholds of hydrocarbon generation under high temperature and high pressure conditions. At 839 K, strong fluorescence appeared in the Raman spectra, indicating the staring of chemical reaction and the formation of conjugated or polycyclic aromatic species (Cloutis et al., 2014) (Fig. 2a). At 941 K, a new peak appeared at 1586 cm^{-1}, which is assigned to G band (Yang et al., 2021). No additional peaks appeared upon further heating to 974 K and remains 2 h, suggesting that the reaction had completed and the system had stabilized. After cooling down to room temperature, the peaks were observed at 1614, 2956 and 3228 cm^{-1}, corresponding to the G, D + G and 2G bands, respectively. This confirms the formation of disordered graphite. Additionally, during decompression at 9.7 GPa, new peaks appeared at 1098 cm^{-1} (C–O stretching) and 3628 cm^{-1} (O–H stretching), both of which disappeared simultaneously upon reaching 0.1 GPa (Fig. 2b). This indicates the presence of volatile alcohols in the reaction products. Notably, the sample chamber wall remained sharp and well-defined with no observable roughening, indicating that the gasket did not interfere with the reaction. Compared to laser heating, resistive heating involves a larger heated volume and longer duration, which may allow generated hydrogen species to diffuse into the gasket and escape from the reaction chamber, resulting in a net loss of hydrogen.

To make an accurate chemical analysis of the gaseous products generated during the reaction, we utilized a multi-anvil apparatus to carry out the experiment at 10 GPa and ~1600 K. The sample was sealed within a Pd-Au capsule. Upon completion of the reaction, the capsule was carefully punctured using a custom-designed gas extraction apparatus (Supplementary Data Fig. S2), and the released gases were analyzed using gas chromatography-mass spectrometry (GC–MS). The result revealed the presence of acetaldehyde and ethanol (Fig. 3a and b), which are obviously the intermediate products in the reduction pathway from carbonate to hydrocarbon. This provides experimental evidence supporting a stepwise reduction mechanism rather than a direct transformation. XRD analysis of the solid residues identified graphite as the predominant products, as shown in Fig. 3c.

4. Discussion

4.1. Pressure–temperature dependency of the production of abiotic hydrocarbon

The laser-heating DAC experiments on the hydromagnesite–Fe O–H_2O system reveal a systematic evolution in hydrocarbon speciation as pressure and temperature increase from upper-mantle to transition-zone and lower-mantle conditions. The experimental results reveal a distinct trend in abiotic hydrocarbon evolution, transitioning from saturated to unsaturated hydrocarbons as pressure and temperature increase from the mantle transition zone to

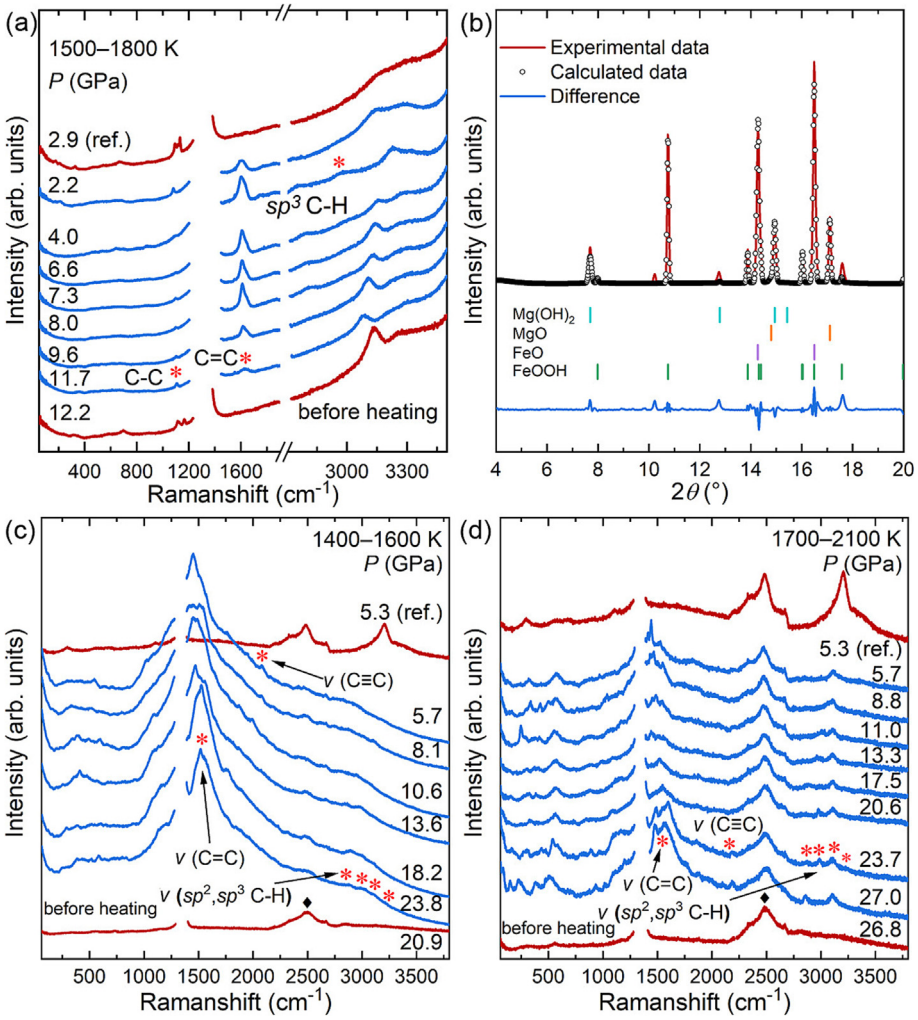

Fig. 1. Raman spectra of the product obtained by heating the system at 1400–2100 K and 12–26.8 GPa during decompression. (a) 12 GPa and 1500–1800 K; the red lines illustrate the spectra of the raw materials before heating at the pressure of 2.9 GPa and 12.2 GPa, using to compare the spectra after heating. New peaks are marked by the asterisks. The second-order Raman peak of diamond was omitted. (b) Rietveld refinement plot of the solid product at 1.8 GPa, λ = 0.6199 Å. Raman spectra of the product obtained at (c) 1400–1600 K, 20.9 GPa and (d) 1700–2100 K, 26.8 GPa. The red lines also represent the spectra of the system before heating at the pressure of 5.3 GPa, 20.9 GPa, and 26.8 GPa. New peaks are marked by the asterisks. *ν*: stretching vibration. The C–H stretching vibrations is decomposed into sp^3 (2850–3000 cm^{-1}; CH_2/CH_3 symmetric and anti-symmetric stretching), sp^2 (3000–3250 cm^{-1}; =C–H stretching). The broad band marked by black rhombus at ~2500 cm^{-1} corresponds to the second-order Raman peak of diamond. arb. units: arbitrary units.

the lower mantle. This is consistent with theoretical predictions and previous experimental findings (Kenney et al., 2002; Spanu et al., 2011; Lobanov et al., 2013; McCollom, 2013). First-principles molecular dynamic simulation has calculated that methane can undergo thermodynamically favorable transformations into advanced alkanes such as ethane and propane, accompanied by the release of H_2 under 2–300 GPa, 800–5000 K (Ancilotto et al., 1997; Kenney et al., 2002; Spanu et al., 2011). As temperature and pressure rise, the system tends to accumulate H_2 and preferentially forms more complex hydrocarbons (Spanu et al., 2011). This thermodynamic tendency has been corroborated by various experimental research. CH_4 was reported to polymerize into C_2H_6 – C_4H_{10} at 2–5 GPa and 1000–1500 K (Kolesnikov et al., 2009), and alkenes, alkynes and unsaturated carbon chains at 10–80 GPa above 1100 K (Hirai et al., 2009; Lobanov et al., 2013), or diamond at 2000–3000 K and 10–50 GPa (Benedetti et al., 1999). These findings indicate a general trend that small organic molecules undergo polymerization or carbonization under high temperature and high pressure conditions (T > 1000 K, P > 2 GPa), resulting in the formation of complex hydrocarbons or carbon-rich species, such as graphite and diamond.

4.2. Stepwise carbonate reduction and the role of alcohol/aldehyde intermediates

Our resistive-heating DAC run at 12 GPa and 974 K provides a complementary perspective at lower temperature. The development of strong fluorescence, followed by the appearance of G, D + G and 2G bands, implies the formation of disordered graphite. This behavior is in line with the notion that, once conjugated π-bonded networks, progressive dehydrogenation under HPHT conditions drives the system toward pure carbon phases. At the same time, peaks at ~1098 and 3628 cm^{-1}, which disappear upon full decompression, are consistent with volatile alcohol species. The coexistence of disordered graphite and alcohols in the quenched products shows that the carbonate–H_2O components have undergone reduction and dehydrogenation. The presence of disordered graphite in the solid products confirms that as $f(H_2)$ decreases due to permeation, the system thermodynamically favors the formation of carbon-rich compounds. This observation aligns with the dehydrogenation-driven carbonization pathway anticipated under *HPHT* conditions. On the other hand, the presence of alcohols in the products suggests that the reduction of carbonate to hydrocarbon may occur through a multi-step mechanism, involving the forma-

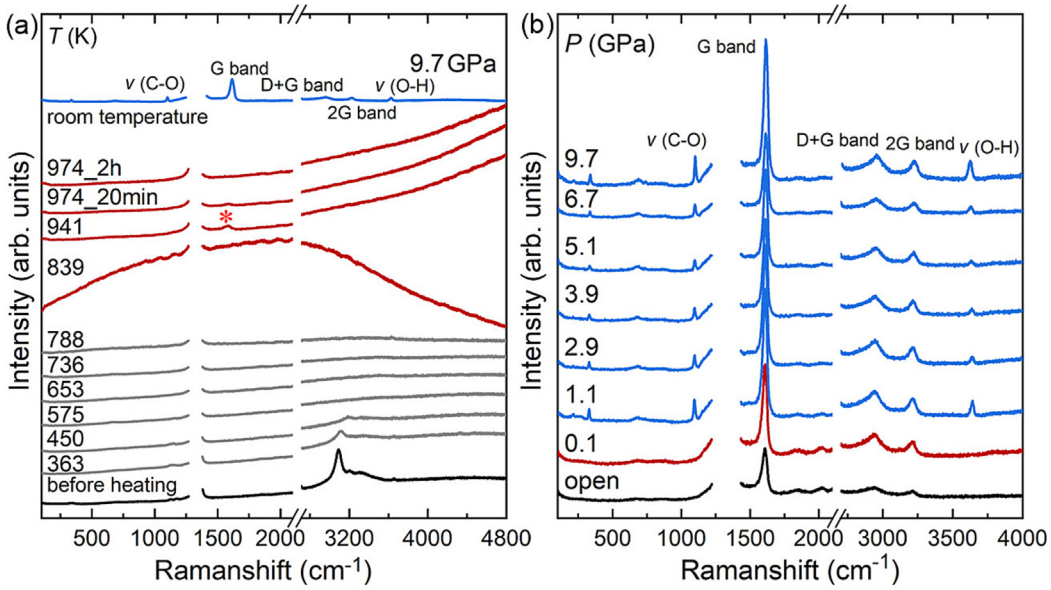

Fig. 2. Raman spectroscopy of the resistance heating experiment. (a) Raman spectra of the system with increasing temperature at 12.0 GPa. The black lines represent the spectra of the raw materials before heating, using to compare the spectra after heating. New peaks are marked by the asterisks. (b) Raman spectra of the products during decompression. *ν*: stretching vibration. The second-order Raman peak of diamond was omitted. arb. units: arbitrary units.

tion of alcohol intermediate prior to further reduction. These findings not only enhance our understanding of abiotic hydrocarbon generation pathways but also imply that hydrocarbon formation in the deep Earth may involve more complex multistage redox processes rather than a single-step transformation pathway. Overall, the combined DAC results indicate that in deep mantle environments, carbonate-derived hydrocarbons are thermodynamically and kinetically predisposed to evolve from saturated molecules toward unsaturated, conjugated and ultimately carbonized products.

In the large-volume multi-anvil experiment at 10 GPa and ~1600 K, GC–MS analysis of the recovered gases identifies ethanol and acetaldehyde, while XRD of the solid residue reveals graphite as the dominant carbon phase. Taken together, these observations support a stepwise reduction pathway in which carbonate-derived oxidized carbon is converted into oxygenated intermediates (alcohols/aldehydes) prior to full deoxygenation and carbonization. Importantly, the coexistence of oxygenated organics and graphite indicates that hydrogen and oxygen are redistributed during reaction progress, rather than directly forming hydrocarbons. These results not only elucidate a potential possible reaction pathway involving carbonate reduction through aldehydes and alcohol intermediates but also underscore the thermodynamic favorability of dehydrogenation-carbonization processes under deep Earth conditions, particularly in the closed or semi-closed systems where hydrogen permeation is facilitated. In the DAC experiments, the hydrogen can diffuse out of the sample chamber into the gasket. The formation of graphite demonstrated that progressive dehydrogenation, which drives the system from alcohol/aldehyde-bearing fluids toward carbon-rich solid products. The differences between the LVP and DAC results are mainly due to the variations in sample volume and detection methods. The multi-anvil press enables larger sample volumes, thereby increasing the quantity of aldehydes (e.g., acetaldehyde) compared with DAC experiments. In contrast, the DAC chamber contains orders-of-magnitude less material, and the signals of minor oxygenated intermediates may fall below detection thresholds of Raman spectrometer, even if they are produced. Importantly, alcohols were detected in both the multi-anvil and DAC experiments, indicating that oxygenated species are not exclusive to the Pd–Au capsule runs and supporting a common reaction pathway involving oxygen-bearing organics. Overall, carbonate reduction proceeds through oxygenated intermediates and evolves toward carbon-rich products under HPHT conditions, while the apparent discrepancies primarily reflect differences in sample size and detection sensitivity, rather than fundamentally different reaction mechanisms.

Through a systematic summary of known abiotic hydrocarbon formation systems, we identify the reduction of carbonate minerals as one of the primary pathways for generating hydrocarbons in transition zone and lower mantle (Kutcherov et al., 2010a, 2010b; McCollom, 2013; Sonin et al., 2014; Mukhina et al., 2017; Tao et al., 2018). Under high pressure and reducing environment, CO_2 generated by the decomposition of carbonates reacts with hydrogen (it is generated by the reduction of H_2O) to gradually transform into hydrocarbons through redox reactions. By combining historical data with the analysis of the products of this experiment (Kutcherov et al., 2010a, 2010b; McCollom, 2013; Sonin et al., 2014; Mukhina et al., 2017; Tao et al., 2018), a compositional diagram of C–H–O system was constructed that delineates the reaction pathway from carbonates to hydrocarbons (Fig. 4). The reduction of carbonates to hydrocarbons is not a one-step process but undergoes a series of complex intermediate transformation processes with alcohols and aldehydes identified as intermediate. These findings not only provide key evidence supporting multistep abiotic hydrocarbon formation but also enhances our understanding of deep Earth carbon cycling, suggesting that the pivotal role of alcohols and aldehydes in regulating deep carbon migration and transformation cannot be ignored.

4.3. Comparison with previous carbonate–fluid experiments and implications for the deep carbon cycle

Tao et al. investigated Fe-bearing carbonates reacting with water at 1–6 GPa and 600–1200 °C, and showed that CH_4, C_2H_6 and C_3H_8, together with graphite and magnetite, can be produced under conditions representative of cold subduction. Their experiments, complemented by observations from natural carbonated eclogites, indicate that Fe-carbonate reduction is an efficient source of abiotic light hydrocarbons in the crust–upper mantle system (Tao et al., 2018).

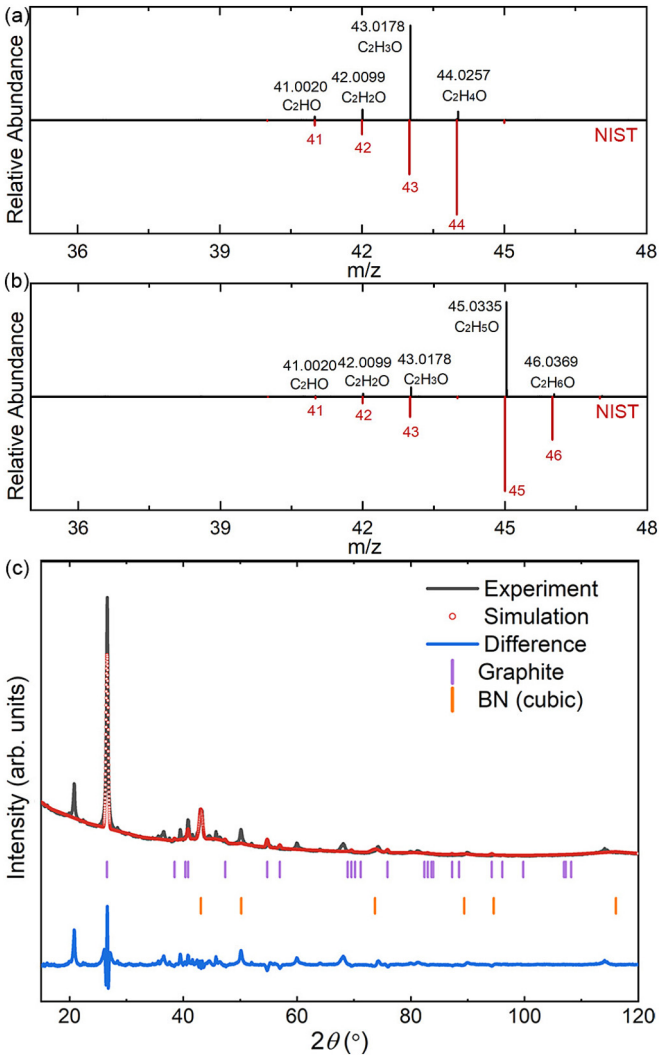

Fig. 3. The products obtained in the large –volume press experiment. (a) and (b): Mass spectrum of the gaseous products. (c) Rietveld refinement plot of the solid product, which indicating the formation of graphite. BN signals originate from the boron nitride parts used in the LVP assembly. NIST: National Institute of Standards and Technology.

Our hydromagnesite–FeO–H_2O experiments presented here extend this framework in three important ways. First, we explore higher pressures and temperatures (10–27 GPa, 900–2100 K), covering the mantle transition zone and lower mantle, thereby demonstrating that carbonate-derived hydrocarbons and carbon-rich phases can also form and evolve in much deeper reservoirs. Second, our system yields not only CH-bearing alkanes but also abundant unsaturated hydrocarbons (olefins and alkynes) and conjugated carbon structures at the higher *P–T* conditions, consistent with the predicted shift from simple molecules toward more polymerized and carbonized products in the deep mantle. Third, the detection of ethanol and acetaldehyde provides evidence for oxygenated intermediates in the reduction of carbonate to hydrocarbons, adding a mechanistic layer that was not captured in most previous studies.

Overall, our study supports a view of the deep Earth in which carbonate reduction, mediated by Fe-bearing minerals and H_2O-rich fluids, can generate not only methane and light hydrocarbons but also a continuum of oxygenated intermediates and carbon-rich solids. This multistage pathway broadens the range of deep carbon reservoirs and transport forms, and refines the mechanistic link

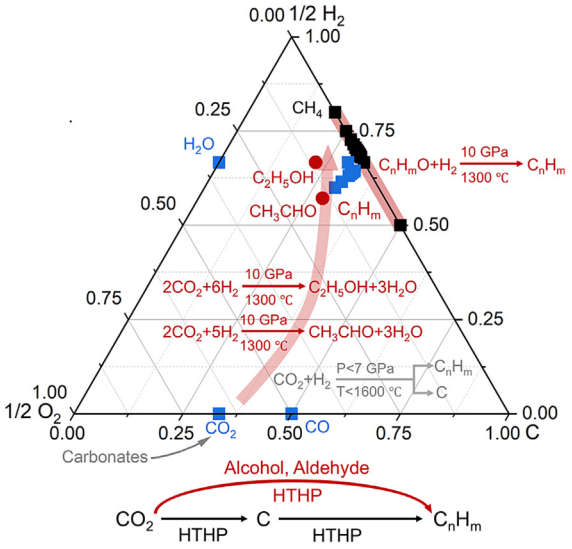

Fig. 4. The compositional diagram of C-H-O system. The black squares represent hydrocarbons, the blue squares represent oxygen-containing compounds, the red circles represent ethanol and acetaldehyde obtained in this experiment. HTHP: high temperature and high pressure.

between subducted carbonates, abiotic hydrocarbons, and carbon-bearing phases stored or recycled in the transition zone and lower mantle.

5. Conclusion

In summary, the experimental investigation demonstrates that $4MgCO_3{\cdot}Mg(OH)_2{\cdot}4H_2O$-FeO-$H_2O$ system could generate a variety of abiotic hydrocarbons under high temperature and high pressure conditions correspond to the Earth's mantle transition zone and lower mantle. Raman spectroscopy, XRD, and GC–MS analyses collectively reveal that as pressure and temperature increase, the hydrocarbon products evolve progressively from saturated alkanes to unsaturated hydrocarbons (alkenes, alkynes) or carbon-rich phases such as graphite. Our results identified disordered graphite, alcohol and aldehyde intermediates, which demonstrates a multistep reduction mechanism, in which carbonates are initially reduced to oxygen-containing compounds (aldehydes or alcohols), followed by deoxygenation to form hydrocarbons. These findings provide compelling experimental evidence for the feasibility of abiotic hydrocarbon formation in the deep Earth. Our research has made significant contributions to a broader understanding of deep carbon reservoirs and highlights the potential for previously unexplored abiotic hydrocarbon sources in Earth's interior.

CRediT authorship contribution statement

Jingqin Xu: Writing – original draft, Investigation. **Yajie Wang:** Investigation. **Dexiang Gao:** Investigation. **Hao Luo:** Investigation. **Jie Zhang:** Investigation. **Yunfan Fei:** Investigation. **Ruyue Shi:** Investigation. **Guoliang Niu:** Investigation. **Ho-kwang Mao:** Funding acquisition. **Kuo Li:** Writing – review & editing. **Haiyan Zheng:** Writing – review & editing.

Declaration of competing interest

The authors declare that they have no known competing financial interests or personal relationships that could have appeared to influence the work reported in this paper.

Acknowledgements

This research was funded by the National Key Research and Development Program of China (2019YFA0708502). The authors express their gratitude for the support received from the National Natural Science Foundation of China (NSFC) under Grant No. 22022101. The high-pressure in situ X-ray diffraction experiments were conducted at the 4W2 HP-Station of the Beijing Synchrotron Radiation Facility (BSRF), 15U1 beamline and BL17UM at Shanghai Synchrotron Radiation Facility. This study was partially supported by Synergetic Extreme Condition User Facility (SECUF).

Appendix A. Supplementary data

Supplementary data to this article can be found online at https://doi.org/10.1016/j.gsf.2026.102294.

References

Ancilotto, F., Chiarotti, G.L., Scandolo, S., Tosatti, E., 1997. Dissociation of methane into hydrocarbons at extreme (planetary) pressure and temperature. Science 275 (5304), 1288–1290.

Benedetti, L.R., Nguyen, J.H., Caldwell, W.A., Liu, H., Kruger, M., Jeanloz, R., 1999. Dissociation of CH_4 at high pressures and temperatures: diamond formation in giant planet interiors? Science 286 (5437), 100–102.

Charlou, J.L., Donval, J.P., Konn, C., Ondréas, H., Fouquet, Y., Jean-Baptiste, P., Fourré, E., 2010. High production and fluxes of H_2 and CH_4 and evidence of abiotic hydrocarbon synthesis by serpentinization in ultramafic-hosted hydrothermal systems on the Mid-Atlantic Ridge. In: Rona, P.A., Devey, C.W., Dyment, J., Murton, B.J. (Eds.), Diversity of Hydrothermal Systems on Slow Spreading Ocean Ridges. Geophysical Monograph Series, American Geophysical Union, Washington, DC, pp. 265–296.

Chen, H.Y., Xiang, S.K., Yan, X.Z., Zheng, L.R., Zhang, Y., Liu, S.G., Bi, Y., 2016. Phase transition of solid bismuth under high pressure. Chin. Phys. B 25 (10), 108103.

Cloutis, E., Szymanski, P., Applin, D., 2014. Raman (532 nm) Spectroscopy of Polycyclic Aromatic Hydrocarbons. In: 45th Annual Lunar and Planetary Science Conference. LPI Contribution, 1777, 1996.

Colin, A., Schmidt, C., Pokrovski, G.S., Wilke, M., Borisova, A.Y., Toplis, M.J., 2020. In situ determination of sulfur speciation and partitioning in aqueous fluid-silicate melt systems. Geochem. Perspect. Lett. 14, 31–35.

Dasgupta, R., Hirschmann, M.M., 2010. The deep carbon cycle and melting in Earth's interior. Earth Planet. Sci. Lett. 298 (1–2), 1–13.

Dasgupta, R., 2013. Ingassing, storage, and outgassing of terrestrial carbon through geologic time. Rev. Mineral. Geochem. 75 (1), 183–229.

Etiope, G., Sherwood Lollar, B., 2013. Abiotic methane on Earth. Rev. Geophys. 51, 276–299.

Farsang, S., Zajacz, Z., 2024. Sulfur species and gold transport in arc magmatic fluids. Nat. Geosci. 18 (1), 98–104.

Frezzotti, M., Selverstone, J., Sharp, Z., Compagnoni, R., 2011. Carbonate dissolution during subduction revealed by diamond-bearing rocks from the Alps. Nat. Geosci. 4 (10), 703–706.

Gleason, A.E., Jeanloz, R., Kunz, M., 2008. Pressure-temperature stability studies of FeOOH using X-ray diffraction. Am. Mineral. 93 (11–12), 1882–1885.

Hirai, H., Konagai, K., Kawamura, T., Yamamoto, Y., Yagi, T., 2009. Polymerization and diamond formation from melting methane and their implications in ice layer of giant planets. Phys. Earth Planet. Inter. 174 (1–4), 242–246.

Hu, Q., Kim, D.Y., Yang, W., Yang, L., Meng, Y., Zhang, L., Mao, H.K., 2016. FeO_2 and FeOOH under deep lower-mantle conditions and Earth's oxygen-hydrogen cycles. Nature 534, 241–244.

Hu, Q., Kim, D.Y., Liu, J., Meng, Y., Yang, L., Zhang, D., Mao, W.L., Mao, H.K., 2017. Dehydrogenation of goethite in Earth's deep lower mantle. Proc. Natl. Acad. Sci. U.S.A. 114 (7), 1498–1501.

Kenney, J.F., Kutcherov, V.A., Bendeliani, N.A., Alekseev, V.A., 2002. The evolution of multicomponent systems at high pressures: VI. The thermodynamic stability of the hydrogen–carbon system: the genesis of hydrocarbons and the origin of petroleum. Proc. Natl. Acad. Sci. U.S.A. 99 (17), 10976–10981.

Kolesnikov, A., Kutcherov, V.G., Goncharov, A.F., 2009. Methane-derived hydrocarbons produced under upper-mantle conditions. Nat. Geosci. 2 (8), 566–570.

Kudryavtsev, D., Serovaiskii, A., Mukhina, E., Kolesnikov, A., Gasharova, B., Kutcherov, V., Dubrovinsky, L., 2017. Raman and IR spectroscopy studies on propane at pressures of up to 40 GPa. J. Phys. Chem. A 121 (32), 6004–6011.

Kutcherov, V.G., 2013. Abiogenic Deep Origin of Hydrocarbons and Oil and Gas Deposits Formation. In: Kutcherov, V., Kolesnikov, A. (Eds.), Hydrocarbon. InTech, Rijeka, pp. 1–28.

Kutcherov, V., Bendeliani, N., Alekseev, V., Kenney, J., 2002. Synthesis of hydrocarbons from minerals at pressures up to 5 GPa. Dokl. Phys. Chem. 387 (4–6), 328–331.

Kutcherov, V., Kolesnikov, A., Dyuzheva, T., Brazhkin, V., 2010. Synthesis of hydrocarbons under upper mantle conditions: evidence for the theory of abiotic deep petroleum origin. J. Phys.: Conf. Ser. 215, 012103.

Kutcherov, V., Kolesnikov, A.Y., Dyuzheva, T., Kulikova, L., Nikolaev, N., Sazanova, O., Braghkin, V., 2010. Synthesis of complex hydrocarbon systems at temperatures and pressures corresponding to the Earth's upper mantle conditions. Dokl. Phys. Chem. 433 (1), 132–135.

Kutcherov, V.G., Krayushkin, V.A., 2010. Deep-seated abiogenic origin of petroleum: from geological assessment to physical theory. Rev. Geophys. 48 (1), RG1001.

Leila, M., Hazlett, R., George, P.M., Šegvić, B., Fustic, M., 2025a. Low temperature carbonation and CO_2 mineral trapping in altered hydrotalcite-rich ultrmafic rocks. Sci. Rep. 15 (1), 31133.

Leila, M., Hazlett, R., George, P.M., Moretti, I., Kabashev, Z., Fustic, M., 2025b. Concomitant generation of hydrogen during carbon dioxide storage in ultramafic massifs-state of the art with implications to decarbonization strategies. Carbon Capt. Sci. Technol. 16, 100481.

Li, Y., Tang, X., Zhang, P., Wang, Y., Yang, X., Wang, X., Li, K., Wang, Y., Wu, N., Tang, M., Xiang, J., Lin, X., Lee, H.H., Dong, X., Zheng, H., Mao, H.K., 2021. Scalable high-pressure synthesis of sp(2)-sp(3) carbon nanoribbon via [4 + 2] polymerization of 1,3,5-triethynylbenzene. J. Phys. Chem. Lett. 12 (30), 7140–7145.

Lobanov, S.S., Chen, P.N., Chen, X.J., Zha, C.S., Litasov, K.D., Mao, H.K., Goncharov, A. F., 2013. Carbon precipitation from heavy hydrocarbon fluid in deep planetary interiors. Nat. Commun. 4, 2446.

Mao, H.K., Hu, Q., Yang, L., Liu, J., Kim, D.Y., Meng, Y., Zhang, L., Prakapenka, V.B., Yang, W., Mao, W.L., 2017. When water meets iron at Earth's core–mantle boundary. Natl. Sci. Rev. 4 (6), 870–878.

Mao, H., Xu, J.A., Bell, P., 1986. Calibration of the ruby pressure gauge to 800 kbar under quasi-hydrostatic conditions. J. Geophys. Res. Solid Earth 91 (B5), 4673–4676.

McCollom, T.M., Bach, W., 2009. Thermodynamic constraints on hydrogen generation during serpentinization of ultramafic rocks. Geochim. Cosmochim. Acta 73 (3), 856–875.

McCollom, T.M., 2013. Laboratory simulations of abiotic hydrocarbon formation in Earth's deep subsurface. Rev. Mineral. Geochem. 75 (1), 467–494.

Molina, J.F., Poli, S., 2000. Carbonate stability and fluid composition in subducted oceanic crust: an experimental study on H_2O–CO_2-bearing basalts. Earth Planet. Sci. Lett. 176 (3–4), 295–310.

Mukhina, E., Kolesnikov, A., Kutcherov, V., 2017. The lower pT limit of deep hydrocarbon synthesis by $CaCO_3$ aqueous reduction. Sci. Rep. 7, 5749.

Pearson, D.G., Brenker, F.E., Nestola, F., McNeill, J., Nasdala, L., Hutchison, M.T., Matveev, S., Mather, K., Silversmit, G., Schmitz, S., Vekemans, B., Vincze, L., 2014. Hydrous mantle transition zone indicated by ringwoodite included within diamond. Nature 507, 221–224.

Petříček, V., Dušek, M., Palatinus, L., 2014. Crystallographic computing system JANA2006: general features. Z. Kristallogr. Cryst. Mater. 229, 345–352.

Prescher, C., Prakapenka, V.B., 2015. DIOPTAS: a program for reduction of two-dimensional X-ray diffraction data and data exploration. High Press. Res. 35 (3), 223–230.

Read, L.Q., Spender, J.E., Proctor, J.E., 2020. Raman spectroscopy of ethane (C_2H_6) to 120 GPa at 300 K. J. Raman Spectrosc. 51 (11), 2311–2317.

Rekhi, S., Dubrovinsky, L.S., Saxena, S.K., 1999. Temperature-induced ruby fluorescence shifts up to a pressure of 15 GPa in an externally heated diamond anvil cell. High Temp. High Press. 31, 299–305.

Scott, H.P., Hemley, R.J., Mao, H.K., Herschbach, D.R., Fried, L.E., Howard, W.M., Bastea, S., 2004. Generation of methane in the Earth's mantle: in situ high pressure–temperature measurements of carbonate reduction. Proc. Natl. Acad. Sci. U.S.A. 101 (39), 14023–14026.

Sharma, A., Cody, G.D., Hemley, R., 2009. In situ diamond-anvil cell observations of methanogenesis at high pressures and temperatures. Energy Fuels 23 (11), 5571–5579.

Song, W., Shan, S., Tang, Q., Su, C., Liu, Y., 2021. Pressure calibration and sound velocity measurement to 12 GPa in multi-anvil apparatus. Acta Geochim. 40, 525–531.

Sonin, V.M., Bul'bak, T.A., Zhimulev, E.I., Tomilenko, A.A., Chepurov, A.I., Pokhilenko, N.P., 2014. Synthesis of heavy hydrocarbons under *P-T* conditions of the Earth's upper mantle. Dokl. Earth Sci. 454, 32–36.

Spanu, L., Donadio, D., Hohl, D., Schwegler, E., Galli, G., 2011. Stability of hydrocarbons at deep Earth pressures and temperatures. Proc. Natl. Acad. Sci. U.S.A. 108 (17), 6843–6846.

Tao, R., Zhang, L., Tian, M., Zhu, J., Liu, X., Liu, J., Höfer, H.E., Stagno, V., Fei, Y., 2018. Formation of abiotic hydrocarbon from reduction of carbonate in subduction zones: Constraints from petrological observation and experimental simulation. Geochim. Cosmochim. Acta 239, 390–408.

Thompson, E.C., Campbell, A.J., Tsuchiya, J., 2017. Elasticity of ε-FeOOH: Seismic implications for Earth's lower mantle. J. Geophys. Res. Solid Earth 122 (7), 5038–5047.

Vitale Brovarone, A., Sverjensky, D.A., Piccoli, F., Ressico, F., Giovannelli, D., Daniel, I., 2020. Subduction hides high-pressure sources of energy that may feed the deep subsurface biosphere. Nat. Commun. 11, 3880.

Wang, C., Tao, R., Walters, J.B., Ren, T., Nan, J., Zhang, L., 2023. Deciphering the origin of abiotic organic compounds on Earth: review and future prospects. Acta Geol. Sin. 97 (1), 288–308.

Ward, M.D., Huang, H.T., Zhu, L., Biswas, A., Popov, D., Badding, J.V., Strobel, T.A., 2018. Chemistry through cocrystals: pressure-induced polymerization of $C_2H_2{\cdot}C_6H_6$ to an extended crystalline hydrocarbon. Phys. Chem. Chem. Phys. 20 (10), 7282–7294.

Xu, J., Lang, P., Liang, S., Zhang, J., Fei, Y., Wang, Y., Gao, D., Hattori, T., Abe, J., Dong, X., Zheng, H., Li, K., 2025. Solid-state Alder-Ene reaction of 1-hexene under high pressure. J. Phys. Chem. Lett. 16 (10), 2445–2451.

Yamawaki, H., 2020. Raman spectroscopy of solid-phase n-dodecane and methyl oleate under high pressure. Spectrochim. Acta A: Mol. Biomol. Spectrosc. 227, 117756.

Yang, X., Li, Y., Wang, Y., Zheng, H., Li, K., Mao, H.K., 2021. Chemical transformations of n-hexane and cyclohexane under the upper mantle conditions. Geosci. Front. 12 (2), 1010–1017.

Zhang, P., Tang, X., Wang, Y., Wang, X., Gao, D., Li, Y., Zheng, H., Wang, Y., Wang, X., Fu, R., Tang, M., Ikeda, K., Miao, P., Hattori, T., Sano-Furukawa, A., Tulk, C.A., Molaison, J.J., Dong, X., Li, K., Ju, J., Mao, H.K., 2020. Distance-selected topochemical Dehydro-Diels-Alder reaction of 1,4-diphenylbutadiyne toward crystalline graphitic nanoribbons. J. Am. Chem. Soc. 142 (41), 17662–17669.